Physica B 183 (1993) 351–362
North-Holland

PHYSICA B

Annealing studies of magnetron-sputtered CoCr thin films

B.G. Demczyk
North Campus Electron Microbeam Analysis Laboratory, University of Michigan, Ann Arbor, MI, USA

J.O. Artman
Data Storage Systems Center, Carnegie Mellon University, Pittsburgh, PA, USA

Received 11 August 1992
Revised 30 October 1992

The microstructure and magnetic properties of annealed CoCr thin films of various thicknesses, deposited on glass substrates, were examined. In general, little grain growth upon annealing was observed. Low-angle grain boundaries, present in as-sputtered films of thickness ≤50 nm, were absent in annealed films. This occurs simultaneously with a decrease in the measured electrical resistivity. A reduction in the in-plane film stress occurs with annealing, correspondingly the experimentally measured anisotropy field values change markedly. A noticeable feature of the microstructure is the appearance of Cr-rich regions in annealed films 50 nm thick and above. These regions are thought to account for the observed increases in the saturation magnetization and coercivity with annealing time.

1. Introduction

CoCr thin films have been proposed for a number of years as candidate materials for perpendicular recording media [1,2]. The enhancement of the magnetic properties of polycrystalline ferromagnetic films via annealing has been reported in the literature for a variety of thin-film materials [3–5]. Fujii et al. [6] and Jong et al. [7] have cited magnetic property (M_s, H_c and K_u) changes upon annealing RF-sputtered CoCr thin films at various temperatures. Mitchell et al. [8] correlated microstructural changes with those observed in the ferromagnetic resonance spectra of annealed RF-sputtered CoCr films. Compositional inhomogeneities were noted by Honda et al. [9] and used to explain the observed magnetic property changes upon annealing in RF-sputtered CoCr films. More recently, Kawanabe et al. [10] and Fartash and Oesterreicher [11] have examined sputtered CoNiTa/Cr and magnetron-sputtered CoCr films, respectively. In the latter work, a model relating M_s to the chromium concentration was proposed. Snyder and Kryder [12] are currently using thermal-magnetic-analysis techniques to investigate magnetic phase separation in annealed CoCr thin films prepared by RF sputtering. The present authors have discussed differences in the microstructure of CoCr films prepared by DC magnetron and RF sputtering [13], the principal difference being the presence of low-angle grain boundaries in the former. The fundamentally different nature of the grain boundaries would be expected to affect consequent microstructural changes with annealing. To date, however, there have been no systematic studies of the simultaneous microstructural and magnetic property variations in annealed DC magnetron-sputtered CoCr films. In addition, although changes in film stress in annealed thin films have been noted [8,14], the contribution to the resulting total anisotropy

Correspondence to: B.G. Demczyk, North Campus Electron Microbeam Analysis Laboratory, University of Michigan, Ann Arbor, MI 48109-2143, USA.

0921-4526/93/$06.00 © 1993 – Elsevier Science Publishers B.V. All rights reserved

field have not been discussed in detail. In this work, we have examined changes in film microstructure and intrinsic stress as well as magnetic properties in annealed CoCr thin films prepared by magnetron sputtering.

2. Experimental

Samples were deposited were at ambient temperature on glass (Corning Type 7059) substrates from a Co–22 at% Cr alloy target by DC magnetron (Varian 'S-gun') sputtering at a rate of ~0.25 nm/s, using an argon pressure of ~1 mTorr. Three film thicknesses were chosen for study: 10 nm, 50 nm and 200 nm. These selections were based on previous studies [15,16], which have shown the magnetization to lie in the film plane in 10 mm thick films, out of the film plane in 200 nm films and to have both in- and out-of-plane component regions in the 50 nm thick films. Annealing was performed at 360°C in a vacuum (10^{-6} Torr) for geometrically incremented times up to a total time of 49 hours. Transmission electron microscopy (TEM) samples were prepared by mechanically thinning the substrates to 40 μm, followed by ion (Ar^+) milling to electron transparency (~50 nm). TEM was performed using a JEOL 2000FX, operating at 200 kV, equipped with an ultra-thin window energy dispersive X-ray detector interfaced to a Tracor-Northern 5502 X-ray microanalysis system. X-ray diffraction (XRD) rocking curves were obtained with a Rigaku Geigerflex diffractometer, using Cu-Kα radiation. Electrical resistivity measurements were made at liquid-nitrogen temperatures, employing a four-point probe technique. In-plane stress values were computed (relative to the as-deposited state) from experimentally measured substrate curvature data. These measurements were made using a cantilever beam technique as described in ref. [17]. Vibrating-sample magnetometry (VSM) was performed (on 49 mm^2 samples) at the Carnegie Mellon University Data Storage Systems Center with a Princeton Applied Research Model 155 vibrating-sample magnetometer. Ferromagnetic Resonance (FMR) measurements were made (on 2 mm^2 samples) on a 33 GHz resonant-cavity system, using a maximum magnetic field of 18 kOe. All magnetic (VSM, FMR), resistivity and stress measurements were made initially (before annealing) and after each annealing increment. X-ray rocking curves and TEM examination were performed initially and after completion of all annealing (i.e. after a total of 49 hours of vacuum annealing).

3. Results and discussion

3.1. Microstructural details

The general microstructure of DC magnetron-sputtered CoCr films has been reported previously [13,18]. Figures 1(a) and (b) show plan view microstructures of a 50 nm thick film in the as-sputtered and annealed (49 hours) state, respectively. The insets show the corresponding [0 0 0 2] selected area electron diffraction (SAD) patterns from the same regions. As shown, there is little change in the observed grain size or in film texture (little difference in the SAD patterns). Table 1 summarizes the film microstructural parameters in a 50 nm thick film before and after annealing (49 hours). No significant grain (or column) growth upon annealing is observed. These results are vastly different from those obtained by Mitchell et al. [8] for annealed RF-sputtered CoCr thin films, in which anomalous grain growth was observed under similar annealing conditions. A slight narrowing of the

Table 1.
Microstructural changes following annealing in vacuum (50 nm thick film).

	As-sputtered	Annealed[e]
d_g [a]	25 (11)	26 (15)
d_c [b]	18–34	18–31
θ_{avg} [c]	12°	20°
$\Delta\theta_{50}$ [d]	9°	8.5°

[a] d_g = average grain (subgrain) diameter, nm.
[b] d_c = column diameter range, nm.
[c] θ_{avg} = average a-axis misorientation.
[d] $\Delta\theta_{50}$ = X-ray rocking curve full width at half maximum.
[e] Total of 49 hours at 360°C, 10^{-6} Torr.

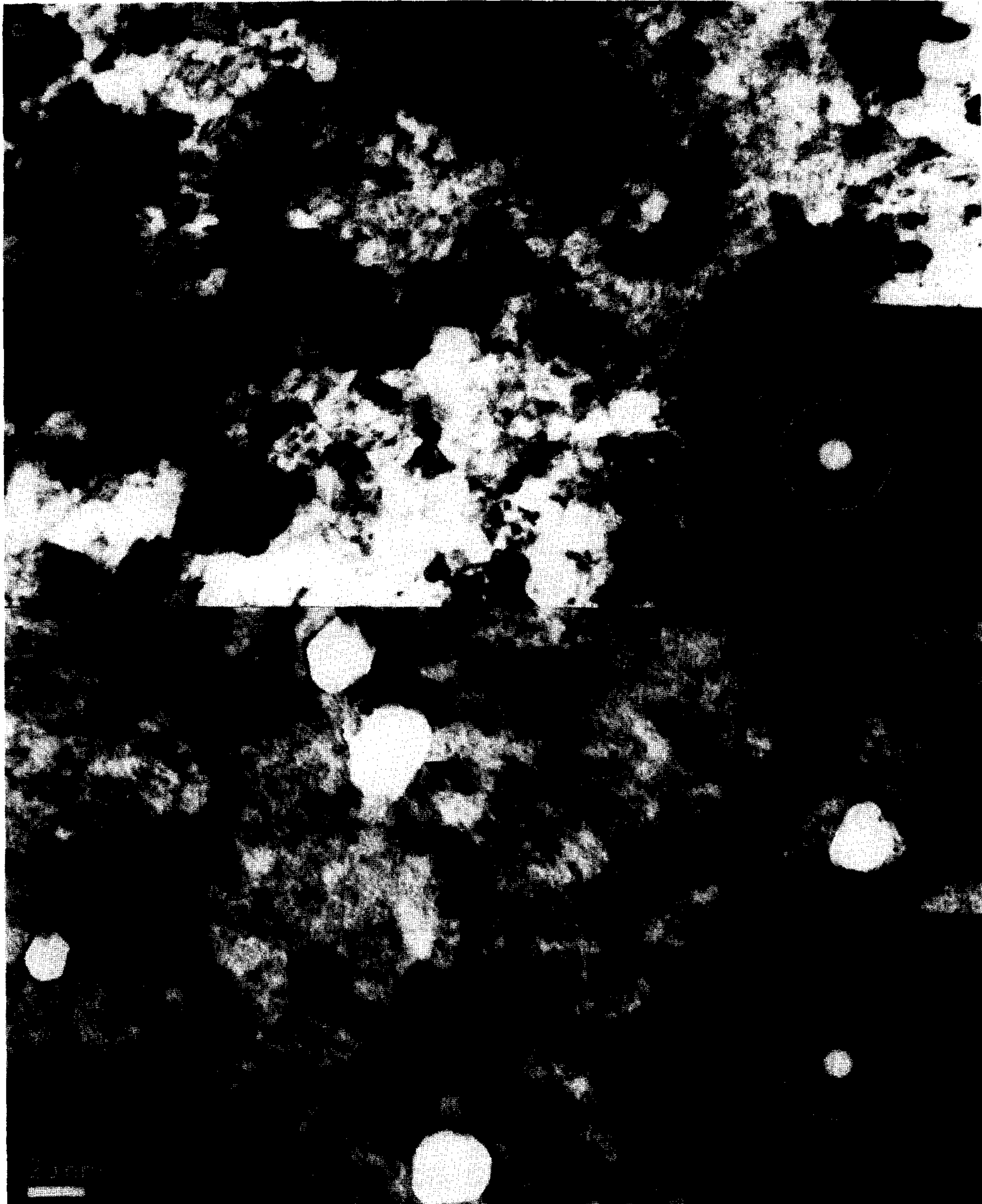

Fig. 1. Plan view transmission electron micrographs of a 50 nm thick CoCr film; (a) as-sputtered; (b) annealed for 49 hours at 360°C. Insets show corresponding selected area diffraction (SAD) patterns from these regions. Note the presence of bright regions in (b) (arrowed).

measured X-ray rocking ($\Delta\theta_{50}$) curve width is noted in the annealed film. More significantly, we find an increase in the average subgrain diameter after annealing. Along with this observation, the average grain-to-grain *a*-axis misorientation (θ_{avg}), measured by random microdiffraction sampling, is found to increase with annealing. As reported previously [13], this parameter decreases when low-angle boundaries (i.e. boundaries across which the HCP *a*-axes lie within 10° of each other) are present. Figures 2(a)–(c) show the experimentally measured resistivity values as a function of annealing time, for films of three different thicknesses. A significant decrease in resistivity in both the 10 and 50 nm thick films with annealing time is found. This is the most pronounced in the 10 nm films which have been shown [13] to initially contain a large number of low-angle boundaries. The resistance of the 200 nm thick film, previously established as having few low-angle boundaries, did not change upon annealing. A resistance decrease was also reported in annealed (600°C) CoPt thin films [19]. The resistance data, along with the increasing grain-to-grain *a*-axis misorientation values following annealing (table 1), suggest the disappearance of low-angle boundaries with annealing.

A notable feature of fig. 1(b) is the presence of bright regions (two are indicated by arrows in fig. 1(b)). Section views (fig. 3(b)) of annealed 50 nm thick films often display cavities (one indicated by an arrow in fig. 3(b)), while they are not found in as-sputtered films (fig. 3(a)). It is believed that these cavities can be correlated with the bright regions, mentioned above (the bright phase, presumably being etched out preferentially by the ion milling operation). Figures 4(a) and (b) display experimentally measured energy dispersive X-ray spectra from a bright region (fig. 4(a)) and from the surrounding matrix (fig. 4(b)), obtained using a nominal 40 nm diameter electron probe. As shown, the bright region is nearly pure Cr, while the surrounding matrix is the expected CoCr alloy. Concurrent work [20] has provided further evidence for Cr redistribution is annealed films. Cr redistribution has also been reported in RF-sputtered CoCr [9] and

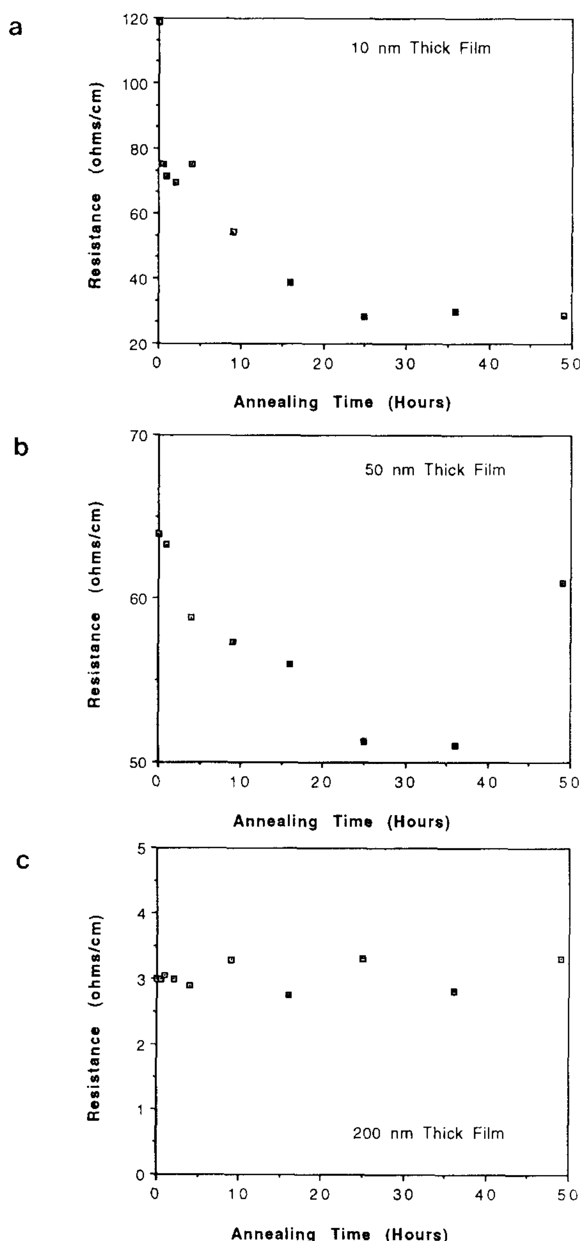

Fig. 2. Electrical resistivity as a function of annealing time (at 360°C) for (a) 10 nm, (b) 50 nm and (c) 200 nm thick CoCr films.

CoNiTa/Cr [10] films annealed at 400°C for 1 hour. In the latter case, it was suggested that Cr migrates to the surface via the grain boundaries. As shown in figs. 5(a) and (b), annealed films of thickness 10 nm do not exhibit the bright phase.

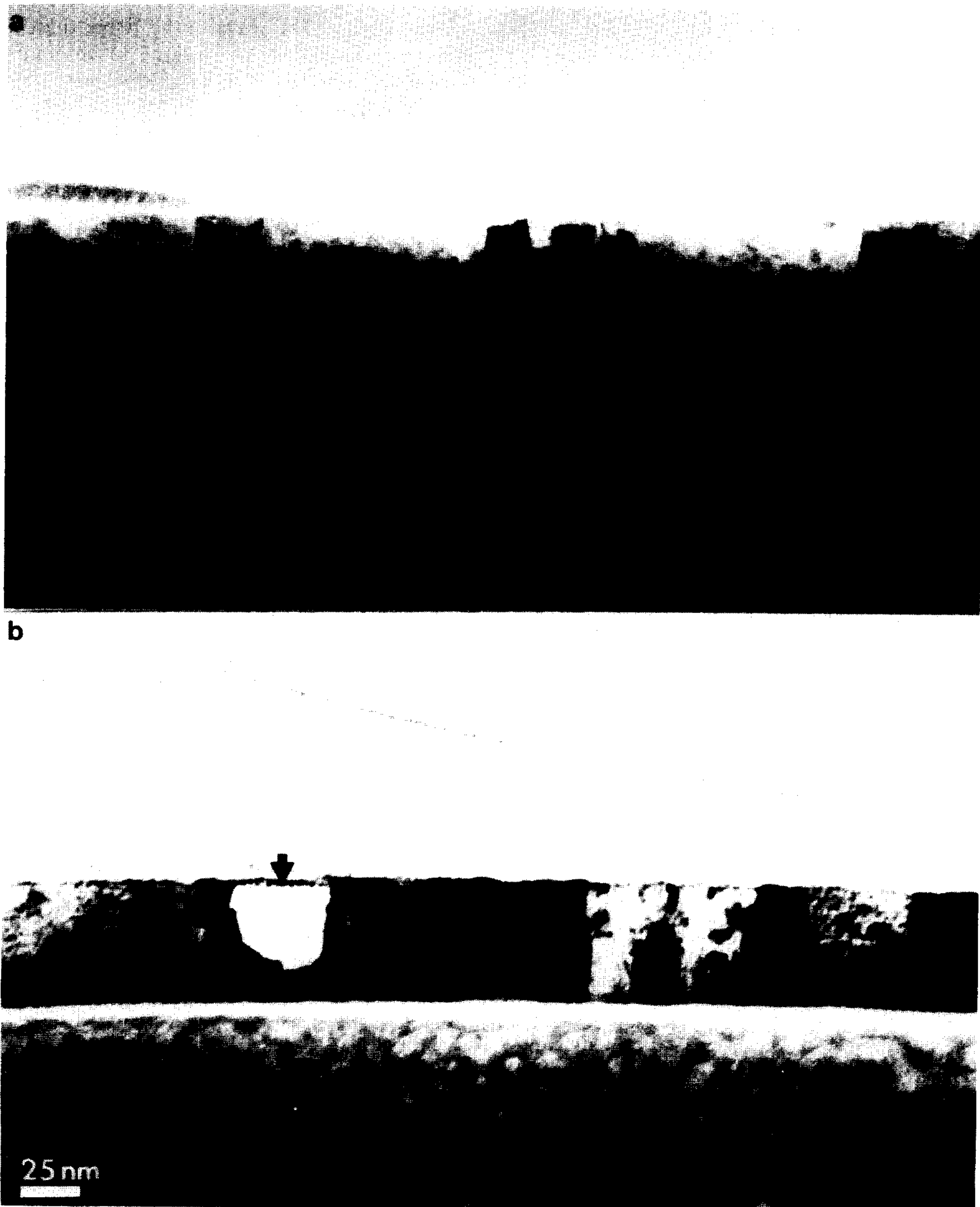

Fig. 3. Section view TEM micrographs of a 50 nm thick CoCr film; (a) as-sputtered; (b) annealed for 49 hours at 360°C. Note the presence of cavities in (b) (arrows).

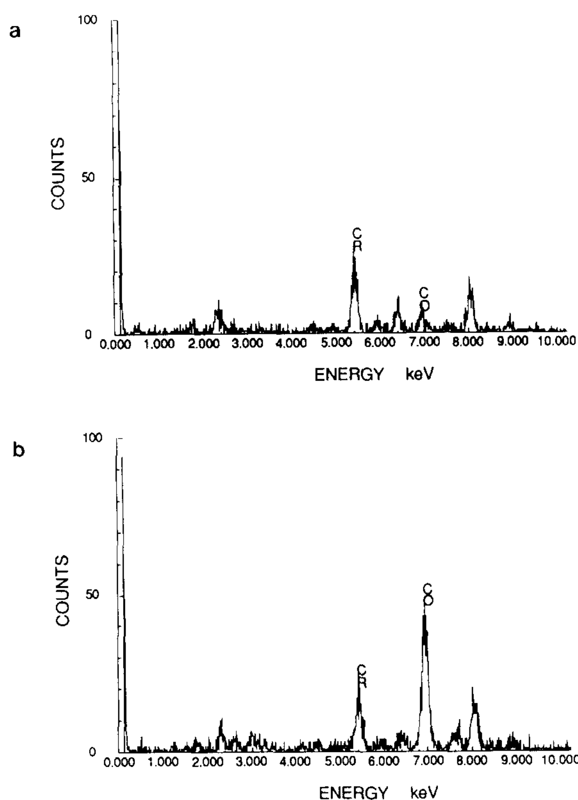

Fig. 4. Energy dispersive X-ray spectra from a 50 nm thick CoCr film annealed for 49 hours at 360°C. (a) Bright region, as per fig. 1(b); (b) surrounding matrix.

As reported previously [13], films of this thickness have not yet developed a columnar microstructure.

3.2. Film stress

Figures 6(a)–(c) show the experimentally determined in-plane film stress as a function of annealing time. As shown, both the 10 nm and the 50 nm thick films exhibit a marked reduction in measured stress with annealing time, especially within the first 16 hours. The 200 nm thick film (fig. 6(c)) shows a much smaller reduction. It is interesting that the stress reduction and the decrease of the electrical resistivity display a similar type of behavior upon annealing. A similar (linear) relationship was found between the measured film stress and the electrical resistivity in sputtered $Al_{0.75}Cu_{0.25}$ [14] films subjected to isothermal aging. The stress in the 10 nm thick films has been previously interpreted to be compressive [16], while that in films of thickness ≥50 nm was found to be tensile [16,21]. We observe a decrease in the magnitude of the stress with annealing time in both cases.

3.3. Magnetic properties

3.3.1. Saturation magnetization

Figures 7(a)–(c) depict experimental values of the total moment ($M_s \times$ volume), where M_s is the saturation magnetization, measured via VSM as a function of annealing time for films of various thickness. In all cases, we observe a steady, albeit decreasing, rise in M_s with annealing time. The data suggest that the increase in M_s is due to a redistribution of Cr with annealing. The value of M_s as measured with the VSM represents an average over a finite volume. Assuming that Cr redistributes to the surface and/or the column boundaries, the bulk of the material sampled by the VSM would be Co-rich, affecting an increase in the measured magnetic moment. Similar results have been reported in RF-sputtered [9,10] CoCr films. This appears to be supported by concurrent X-ray photoelectron spectroscopy studies on these same films [20] as well as the presence of Cr-rich regions at the column boundaries, as discussed above.

3.3.2. Anisotropy field

General comments. Figures 8(a)–(d) depict the effective anisotropy field values, as determined by FMR, plotted as a function of annealing time. The effective anisotropy field, $H_{k\,\mathrm{eff}}$, can be written in terms of its constituent anisotropy field components, as

$$H_{k\,\mathrm{eff}} = \frac{2K_u}{M_s} - \frac{3\sigma\lambda_s}{M_s} - 4\pi M_s \quad (1)$$

where the terms represent the magnetocrystalline, the stress-produced (i.e. inverse magnetostrictive effect) and the shape anisotropy fields, respectively. In eq. (1), K_u represents the uniaxial anisotropy constant, σ the in-plane film

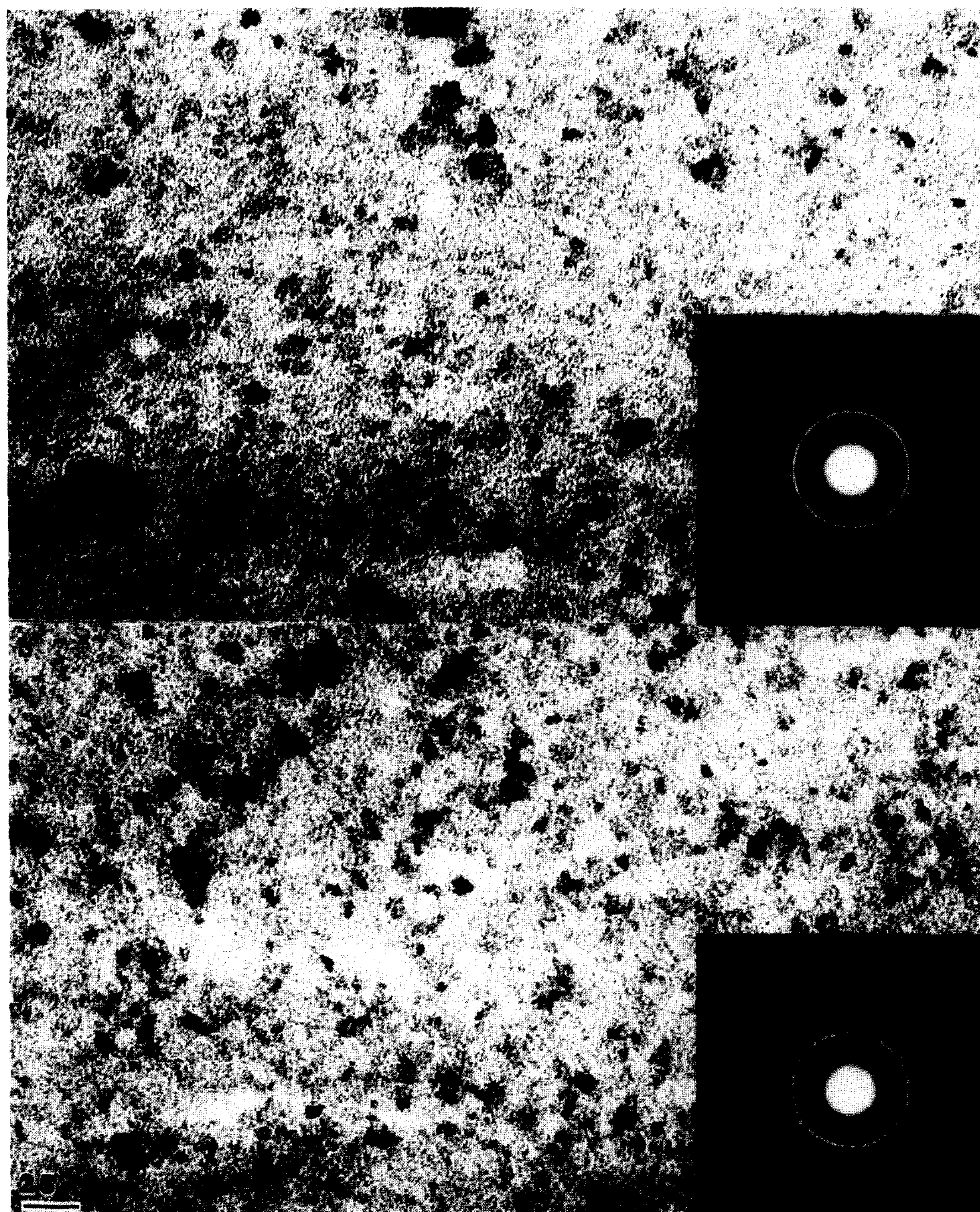

Fig. 5. Plan view TEM micrographs from a 10 nm thick CoCr film; (a) as-sputtered; (b) annealed for 49 hours at 360°C. The insets show the corresponding SAD patterns. Note the absence of bright regions in (b).

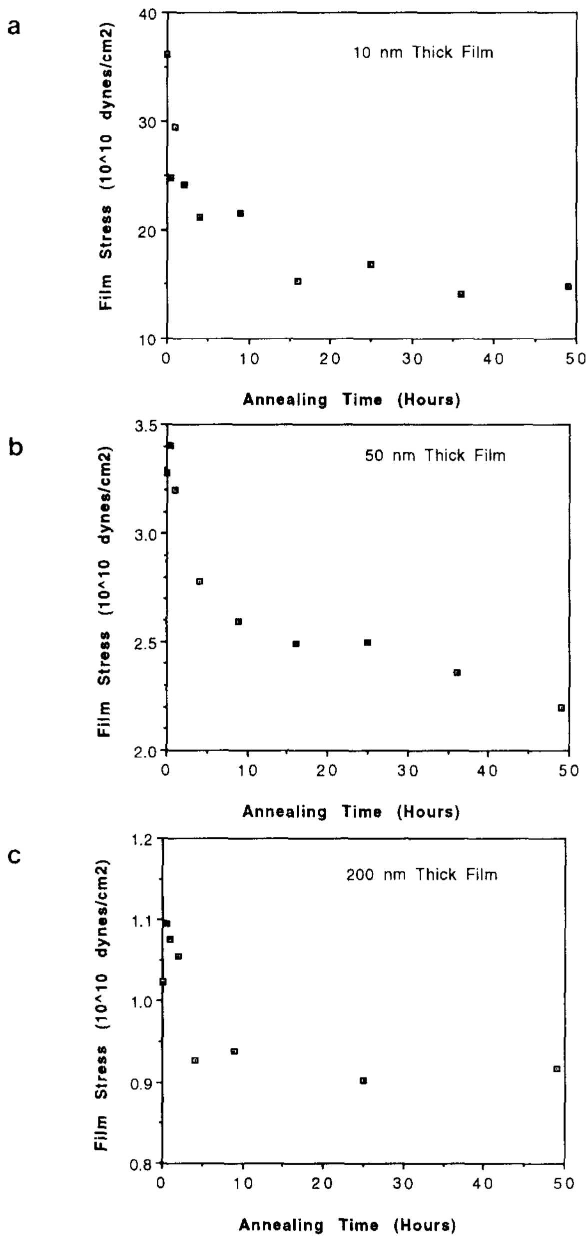

Fig. 6. In-plane film stress as a function of annealing time (at 360°C) for (a) 10 nm, (b) 50 nm and (c) 200 nm thick CoCr films.

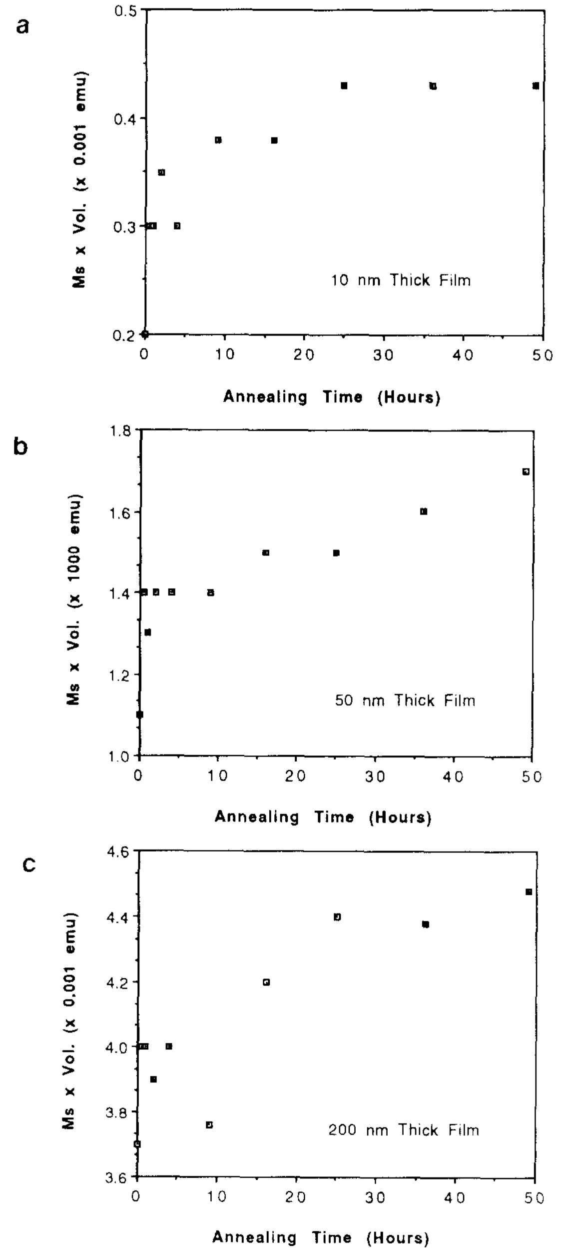

Fig. 7. Saturation magnetization as a function of annealing time (at 360°C) for (a) 10 nm, (b) 50 nm and (c) 200 nm thick CoCr films.

stress, λ_s the saturation magnetostriction and M_s the saturation magnetization, as above. The contribution of each term to the effective anisotropy field has been discussed in detail previously [16,21]. It has been shown [15,16] that, in 5 nm thick CoCr films, the effective anisotropy field is negative, corresponding to in-plane magnetization being energetically favored, while in 200 nm films it is positive (magnetization favored out of the film plane). In 50 nm thick CoCr films, dual

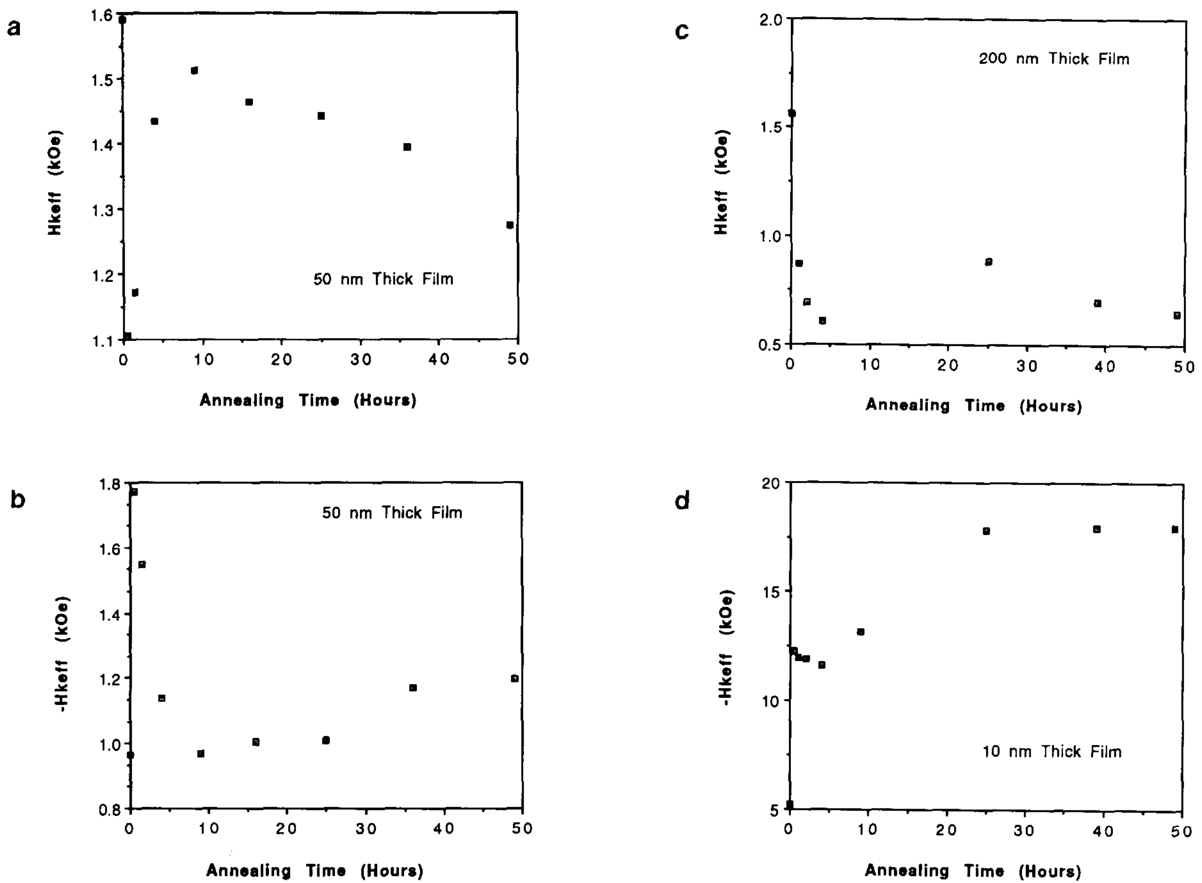

Fig. 8. Effective anisotropy field of CoCr films plotted as a function of annealing time (at 360°C). (a) Positive, (b) negative field for 50 nm thick film; (c) positive field for 200 nm thick film; (d) negative field for 10 nm thick film.

FMR resonances, corresponding to both positive and negative anisotropy fields (in- and out-of-plane magnetization constituents) are present.

50 nm thick film. Referring to fig. 6(b), we observe an initial sharp drop in the measured film stress, followed by a quasi-exponential reduction with annealing from the as-deposited state. After the final anneal, the stress has been reduced to a value of ~0.6 of the initial value. In fig. 7(b) we find that M_s also undergoes a sharp increase (1.3 times the initial value) and then increases gradually more slowly with annealing time (to a value of 1.6 times the initial value at 49 hours total annealing time). In fig. 8(a) the positive effective anisotropy field is plotted as a function of annealing time. We observe an initial large drop, then a subsequent increase, followed by a decrease with annealing time. The magnitude of the negative anisotropy field for this film (fig. 8(b)) exhibits essentially the inverse behavior, with a large initial increase, followed by a decrease, then a gradual increase until it levels off.

Our discussion of these results will be based on eq. (1). We will make several assumptions in the discussion that follows. First, we assume that M_s has the same value throughout the film thickness. As mentioned in ref. [16], we have not found experimental evidence to the contrary. We also take σ to be constant through the film thickness, although we have no direct measurement of this. We also assume that λ_s is negative and does not vary upon annealing; the changes in λ_s with annealing are unknown.

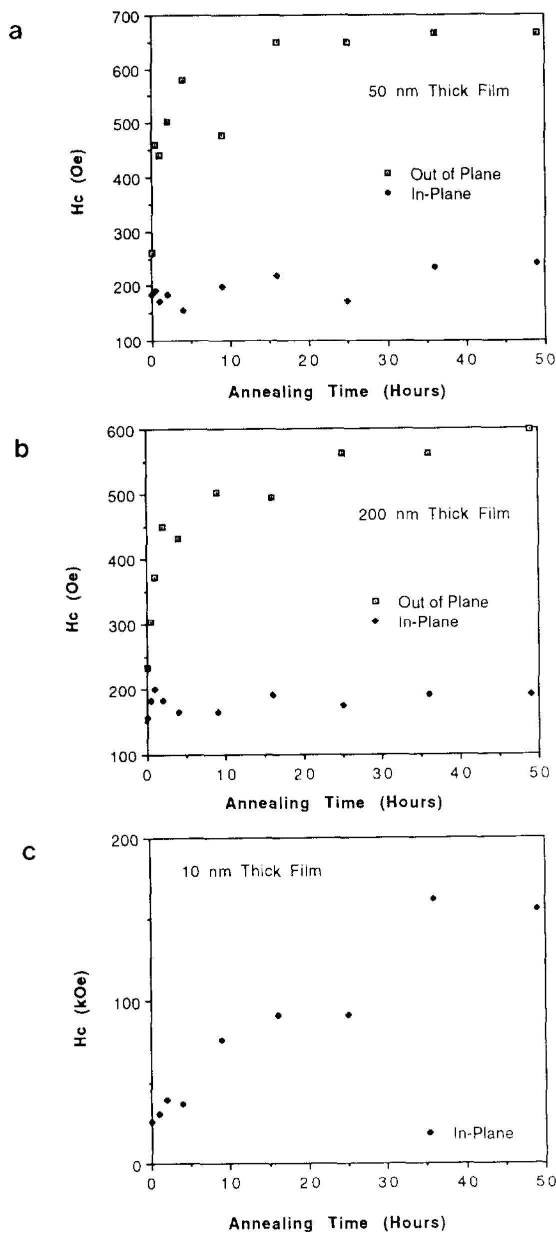

Fig. 9. Coercivity as a function of annealing time (at 360°C) for (a) 50 nm, (b) 200 nm and (c) 10 nm thick CoCr films.

(i) Positive anisotropy field constituent. With the above in mind, we now can examine each term in eq. (1). From the shape anisotropy term ($-4\pi M_s$), an increase in the magnitude of M_s will render $H_{k\,\mathrm{eff}}$ more negative. The magneto-elastic anisotropy field term ($-3\lambda_s\sigma/M_s$) would become less positive for a decrease in (positive) σ and/or an increase in M_s. The dependence of the magnetocrystalline anisotropy field term ($2K_u/M_s$) on annealing is not known. However, Fujii et al. [6] and Honda et al. [9] have found a relationship of the form $(2K_u/M_s) \sim (M_s)^{0.5}$ in annealed RF-diode sputtered CoCr films. If we presume that trend, then the ($-3\lambda_s\sigma/M_s$) and the ($-4\pi M_s$) terms override ($2K_u/M_s$) and $H_{k\,\mathrm{eff}}$ would decrease due to the large initial 'spike' (fig. 8(a)). Subsequently, M_s increases at a slower rate, while σ still decreases sharply. Therefore, the change in the σ/M_s contribution reflects the drop in σ as ($2K_u/M_s \sim M_s^{0.5}$) doesn't change significantly. Overall then, the ($-4\pi M_s$) term renders $H_{k\,\mathrm{eff}}$ more negative, ($-3\lambda_s\sigma/M_s$) less positive (for $\sigma\lambda_s < 0$) and ($2K_u/M_s \sim M_s^{0.5}$) more positive, although the latter is a weak effect after the initial M_s 'spike'. Therefore, with increasing annealing time, $H_{k\,\mathrm{eff}}$ becomes less positive.

(ii) Negative anisotropy field constituent. In this case, previous workers have presumed that the ($2K_u/M_s$) term 'averages out' to zero [15]. Then, from eq. (1), the shape anisotropy field term ($-4\pi M_s$) gives rise to a more negative $H_{k\,\mathrm{eff}}$ (from increasing M_s), whilst the magneto-elastic anisotropy field term ($-3\lambda_s\sigma/M_s$) renders $K_{k\,\mathrm{eff}}$ less positive (for λ_s negative). Initially, we find a negative 'spike' in $H_{k\,\mathrm{eff}}$ (fig. 8(b)) due to the dominant ($-4\pi M_s$) term. Thereafter, the overall trend is for $H_{k\,\mathrm{eff}}$ to become more negative with annealing time after the initial 'spike', albeit at a slower and slower rate.

200 nm thick film. In this case (fig. 8(c)) there is only one predominant resonance, corresponding to a positive $H_{k\,\mathrm{eff}}$. The general trend of the magnitude of $H_{k\,\mathrm{eff}}$ with annealing time is an initial sharp decrease, followed by a slight increase, then a decrease. These trends can be explained in a similar manner as those for the positive anisotropy field resonances in the 50 nm thick film (fig. 8(a)). Thus, the ($-4\pi M_s$) term renders $H_{k\,\mathrm{eff}}$ more negative, ($-3\lambda_s\sigma/M_s$) less positive and ($2K_u/M_s$) more positive. As a consequence, $H_{k\,\mathrm{eff}}$ becomes less positive overall.

10 nm thick film. Like the 200 nm thick-film case, 10 nm thick films also display only one

predominant resonance, this time corresponding to a negative $H_{k\,\mathrm{eff}}$. The general trend of $H_{k\,\mathrm{eff}}$ as a function of annealing time (fig. 8(d)) involves an initial 'spike' (large increase in negative $K_{k\,\mathrm{eff}}$), followed by a more gradual increase out to about 25 hours total annealing time, after which no subsequent changes are noted. Referring to fig. 6(a) we note that σ decreases in magnitude at first sharply and then at a decreasing rate with annealing, while M_s (fig. 7(a)) displays a similar trend in increasing with magnitude with annealing time.

As noted above and in previous work [16] σ has been inferred to be compressive (<0) for these films. Now, again presuming λ_s to be negative we see that the magnetoelastic anisotropy term $(-3\lambda_s\sigma/M_s)$ will tend to make $H_{k\,\mathrm{eff}}$ more negative with an increase in the magnitude of σ and/or a decrease in M_s. Since σ in fact becomes less negative (fig. 6(a)), whilst M_s increases (fig. 7(a)), $H_{k\,\mathrm{eff}}$ should become less negative, in contrast to what is actually observed experimentally (fig. 8(d)). The shape anisotropy field term $(-4\pi M_s)$ will render $H_{k\,\mathrm{eff}}$ more negative for increasing M_s, as is consistent with the data. The presence of initial 'spikes' in all three quantities (σ, M_s and $H_{k\,\mathrm{eff}}$) would argue for a strong magnetoelastic anisotropy field term dependence. The data can be explained if, in fact, λ_s was positive, as was concluded by Mitchell et al. [21] in RF-sputtered CoCr thin films.

3.3.3. Coercivity

Figures 9(a)–(c) show the in- and out-of-plane coercivities as a function of annealing time for films of various thickness. From figs. 9(a) and (b) the out-of-plane coercivity increases with annealing time for both the 50 and 200 nm thick films. The rate of increase diminishes with time, and H_c approaches a constant at ~16 hours for both films. It is to be noted that the in-plane coercivity does not increase under the same annealing conditions. We have previously indicated [16] that the out-of-plane coercivity depends largely on $2K^*/M$ (where $2K^*/M_s = H_{k\,\mathrm{eff}} + 4\pi M_s$) for films $\geqslant$50 nm thick, which is typical of a rotation rather than a wall motion magnetization reversal mechanism. In ref. [9], a relationship between the perpendicular coercivity and the saturation magnetization of the form $H_c \sim M_s^{3.5}$ was found in annealed 50 nm thick RF-diode sputtered CoCr films. It has also been shown [22] that the domain size in films of $\geqslant$50 nm thickness was of the order of the column diameter, each column being comprised of grains or grain clusters separated from surrounding columns by high-angle ($>10°$) boundaries. Thus, it is plausible that the coercivity increases as nonferromagnetic Cr redistributes to the grain boundaries, effectively decoupling the grains. Fujii et al. [6] and Honda et al. [9] attribute the increase in perpendicular coercivity in air-annealed CoCr thin films to the formation of nonferromagnetic Cr_2O_3, surrounding the column boundaries. This issue is the subject of concurrent research [20].

The in-plane magnetization reversal has elsewhere been shown to involve wall motion [16,22]. In-plane domains were observed [22] to be much larger in width ($\geqslant$100 nm) than the average grain size (~20 nm). The principal effect of annealing on the microstructure was shown above to be the removal of small-angle grain boundaries. Concurrent domain nucleation studies have revealed that these boundaries do not act as domain wall barriers [22]. It is thus reasonable that the in-plane coercivity does not change appreciably with annealing (figs. 9(b) and (c)). In the case of the 10 nm thick film (fig. 9(c)), we do observe an increase in the in-plane coercivity with annealing time. It is proposed that, in this case, Cr redistribution causes a large volume of the film to become nonferromagnetic, resulting in a considerable inhibition to domain wall motion, effectively raising H_c. This matter is presently being investigated.

4. Summary

The primary effect of annealing on the microstructure of magnetron-sputtered CoCr thin films was found to be the removal of low-angle boundaries. Cr-rich regions were observed in annealed films possessing a columnar grain morphology. This Cr redistribution with annealing is believed to account for the experimentally observed in-

creases in both M_s and H_c in annealed films. The combination of the reduction in magnitude of the in-plane film stress and the increase in M_s after annealing is thought to give rise to the observed variations in the effective anisotropy field. Overall, data were consistent with primarily domain wall motion magnetization reversal for in-plane applied fields and rotation for fields applied out of the film plane.

Acknowledgements

The authors wish to thank Prof. L. Berger of the Physics Department at Carnegie Mellon University for the use of the electrical-resistivity measurement instrumentation and Prof. C.L. Bauer of the Department of Metallurigical Engineering and Materials Science at Carnegie Mellon for the use of the thin-film stress measurement apparatus. The assistance of K. Rook and J. Cirra in obtaining portions of the magnetic and resistivity data is also gratefully acknowledged. In addition, we thank Dr. K. Hono, presently at Tohoku University, for stimulating discussions resulting in a re-examination of the data in the light of Cr redistribution considerations. Samples were prepared at Carnegie Mellon under a grant from the Division of Materials Research, National Science Foundation, Grant No. DMR-8613396, consequently the government may have certain rights to this material.

References

[1] S. Iwasaki and Y. Nakamura, IEEE Trans. Mag. 13 (1972) 1272.
[2] T. Wielinga, PhD Dissertation, Twente University of Technology, 1983.
[3] C.D. Graham Jr., in: Magnetic Properties of Metals and Alloys, ed. R.M. Bozorth (ASM, Cleveland, OH, 1959) pp. 288–290.
[4] M. Prutton, Thin Ferromagnetic Films (Butterworths, Washington, DC, 1964) pp. 124–127.
[5] T. Sambongi and T. Mitui, J. Phys. Soc. Jpn. 18 (1963) 1253.
[6] Y. Fujii, K. Tsutsumi, T. Numata and Y. Sakurai, J. Appl. Phys. 55 (1984) 2266.
[7] P.W. Jong, T.D. Lee, Y.H. Kim and T. Kong, IEEE Trans. Mag. 26 (1990) 1623.
[8] P.V. Mitchell, A. Layadi, K.R. Mountfield, C. Hwang, J.E. Snyder and J.O. Artman, J. Magn. Magn. Mater. 54–57 (1986) 1701.
[9] S. Honda, N. Yamashita, M. Ohkoshi and T. Kusuda, IEEE Trans. Mag. 20 (1984) 791.
[10] T. Kawanabe, K. Hasegawa, S. Ono, S. Nakagawa and M. Naoe, IEEE Trans. Mag. 26 (1990) 42.
[11] A. Fartash and H. Oesterreicher, J. Appl. Phys. 66 (1989) 3275.
[12] J.E. Snyder and M.H. Kryder, in preparation.
[13] B.G. Demczyk, J. Magn. Magn. Mater. 102 (1991) 239.
[14] A.G. Dirks and J.J. van den Broek, Acta Metall. 37 (1989) 9.
[15] P.V. Mitchell, A. Layadi, N.S. Van der Ven and J.O. Artman, J. Appl. Phys. 57 (1985) 3976.
[16] B.G. Demczyk and J.O. Artman, J. Phys. D 24 (1991) 1627.
[17] D.W. Young, H.L. Ho, C.L. Bauer, S. Mahajan and A.G. Milnes, in: Mat. Res. Soc. Sym. Proc. Vol. 122 (Materials Research Society, Pittsburgh, PA, 1988) p. 573.
[18] J.W. Lee, B.G. Demczyk, K.R. Mountfield and D.E. Laughlin, IEEE Trans. Magn. 23 (1987) 2455.
[19] J.A. Aboaf, S.R. Herd and E. Klokholm, IEEE Trans. Mag. 19 (1983) 1514.
[20] B.G. Demczyk, in preparation.
[21] P.C. Mitchell, K.R. Mountfield and J.O. Artman, J. Appl. Phys. 63 (1988) 2917.
[22] B.G. Demczyk, IEEE Trans. Mag. 28 (1992) 998.